

Carbon nanotubes–metal nitride composites: a new class of nanocomposites with enhanced electrical properties

Linqin Jiang^{ab} and Lian Gao^{*ab}

Received 25th June 2004, Accepted 20th September 2004

First published as an Advance Article on the web 13th October 2004

DOI: 10.1039/b409682g

The fabrication and electrical property characterization of a new class of carbon nanotube (CNT)–nitride nanocomposites have been reported in this work. Electrical property measurements clearly reveal obvious increases in the electrical conductivities confirming the formation of a true composite material with enhanced electrical characteristics. Moreover, the CNT–nitride nanocomposite still retains the electrochemical stability of the nitride material in highly corrosive electrolytes. Nitride nanoparticle-attached CNTs are crucial for the formation and enhanced properties of the composite, which provide good combination and form bridges between CNTs and the nitride matrix to give CNT–nitride composites.

Introduction

There is growing interest in the fabrication and property characterization of CNT-combined composites since the bulk production of multiwalled carbon nanotubes (MWNTs) has become possible and practical.^{1–7} Carbon nanotubes, owing to their excellent electrical conductivity, nonlinear optical properties, and superior mechanical strength, have been widely used in composites with the hope of delivering CNT properties to a processable and synergistic host.^{4,8} In particular, the remarkable electrical properties exhibited by CNTs have already attracted much attention of aiming to combine CNTs with composites to form nanoelectronic elements. Theoretical and experimental results show superior electrical properties of CNTs: electric-current-carrying capacity 1000 times higher than copper wires.⁹ Therefore, it can be foreseen that CNTs could be used as additives to improve electrical properties of nanocomposite materials.¹⁰

In recent years, a lot of research work has concentrated on the use of CNTs as conductive fillers in polymer, metal, or metal oxide matrices to develop their applications in nanoelectronic devices.^{1–7} Chen *et al.* followed an electrochemical route to the formation of CNTs/polypyrrole(PPy), which may have potential applications in CNT-based nanoelectronic structures.¹ Zengin *et al.* reported a study of CNTs/polyaniline(PANI), which increased an order of magnitude in electrical conductivity over that of neat PANI.⁴ In addition, CNT/metal or CNT/metal oxide composites have also been synthesized for improved electrical conductivity.^{5–7,11,12} Xu *et al.* fabricated CNT/Al composites, which slightly increase the electrical conductivity with increasing volume fraction of the nanotubes in aluminium.⁶ Peigney *et al.* used the high-temperature extrusion technique to align CNTs in bulk ceramic-matrix nanocomposites, and the resulting materials show an anisotropy of the electrical conductivity.¹¹ Our previous work employed a simple solvothermal method for the synthesis *in situ* of a CNT–magnetite nanocomposite with

strengthened electrical properties.¹² These studies suggested that CNTs have an obvious effect on the enhancement of electrical properties in a variety of CNT-combined composites.

However, no study concerning the fabrication and electrical properties of CNT–nitride composite has been reported up to the present. Metal nitrides are also promising type of material because of their excellent attributes used in a wide range of applications requiring good electrical properties. They have assumed an important role for employment in advanced microelectronic devices.^{13,14} For example, titanium nitride (TiN) has attracted much interest to be employed as an electrode in electrochemical capacitors,¹⁵ and as an electronic conductor in electronic devices.¹⁶ Iron nitride (Fe_xN) is a new type of electronic ceramic material in the electrical industry.¹⁷ It is expected that CNTs could offer tremendous opportunities for the development of the electrical properties of a new class of CNT–nitride materials. In this report, CNT–TiN and CNT–Fe₂N nanocomposites were successfully fabricated and characterized. Moreover, the electrical and electrochemical properties, as well as the microstructures, of the CNT–nitride nanocomposites have been investigated. This study would help to develop a new class of CNT–nitride composites with enhanced electrical properties employed in CNT-based electronic devices.

Experimental

Multiwall carbon nanotubes prepared by the catalytic decomposition of CH₄¹⁸ were kindly provided by Shenzhen Nanoport company. They were washed in concentrated acids to remove the catalytic metals effectively. CNTs were oxidized by refluxing at 140 °C in concentrated nitric acid for 24 h. After centrifugation, the product was washed with distilled water. Finally, we obtained the precipitate of acidic CNTs by further drying.

The preparation method of nanocrystalline titania has been reported previously.¹⁹ Tetra-butyl titanate [Ti(OC₄H₉)₄], used as a starting material, was dissolved in anhydrous ethanol to form a 10 vol% solution. The mixed solution was added

*liangaoc@online.sh.cn

dropwise into the distilled water with vigorous stirring until the final Ti : H₂O molar ratio reached 1 : 150. The hydrolyzate was filtered and rinsed twice with anhydrous ethanol, then dried at 120 °C for 12 h. The precipitate was subsequently calcinated at 450 °C for 2 h. The nanocrystalline TiO₂ powder was loaded into a quartz boat and heated in flowing NH₃ (0.5 L min⁻¹) at 800 °C for 5 h in a tube furnace to obtain TiN. For preparation of the CNT–TiN nanocomposite, 0.2 g of acidic CNTs were dispersed in distilled water by ultrasonication. The mixed solution of Ti(OC₄H₉)₄ and ethanol was dripped into the stirred suspension containing acidic CNTs. After further rinsing and drying, the Ti precursor with CNTs was calcinated at 450 °C for 2 h in an N₂ atmosphere. Through the same nitride treatment, the CNT–TiN composite was obtained.

To illustrate the combination between CNTs and Ti precursors, zeta potential, FTIR and AES measurements were employed. The zeta potential of the mixed solution containing CNTs and Ti(OC₄H₉)₄ (0.01 wt%) was measured with a Zetaplus analyzer (Zetaplus, Brookhaven, NY, USA). Infrared and XPS analyses were made on an FTIR spectrophotometer (Bio-Rad FTS-185, Hercules, CA) and an X-ray photoelectron spectrometer (Microlab-310F, VG Scientific Ltd., England), respectively.

Iron nitride powder was synthesized from the precursor Fe(III)-urea complex, which was prepared on the basis of a previous reference.²⁰ Anhydrous iron(III) chloride (FeCl₃) was dissolved in anhydrous ethanol to obtain a concentrated solution. Then the solution was dripped into a saturated urea-ethanol solution at 75–80 °C with stirring, until the final salt : urea molar ratio reached 1 : 6. The reaction gave water-soluble precipitation of the Fe(III)-urea complex, Fe[OC(NH₂)₂]_xCl₃, which was separated by filtering. The structure of the complex can be proposed from FTIR studies and previous references.¹⁸ Through the measurement, particularly by the absence of a carbonyl band at 1684 cm⁻¹, and by the decrease in wavenumber of the ν(CO) + σ(NH₂) vibration from 1600 to 1565 cm⁻¹, the formation of oxygen-to-metal coordinate bonds (C=O → Fe) in the Fe-urea complex is determined.^{20–22} In the structure of this complex, the C=O group of urea coordinates with Fe, while –NH₂ groups are located on the outside. The precursor was put into a quartz boat and nitrated at 800 °C for 5 h in a flow of NH₃ gas (0.5 L min⁻¹) using a tube furnace to achieve Fe₂N. For preparation of the CNT–Fe₂N composite, 0.2 g acidic CNTs was sonicated in the mixed solution of urea-ethanol by ultrasonication. A similar procedure was carried out to obtain the CNT–Fe₂N composite.

The composite powders without and with CNTs were pressed into ϕ6 × 1 mm pellets by applying 30 N forces. After cold isostatic pressing at 200 MPa, they were sintered at 900 °C for 2 h in an N₂ atmosphere for titanium nitride composites and in an NH₃ atmosphere for iron nitride composites, respectively, because the Fe₂N composite would decompose in an N₂ atmosphere.

The X-ray diffraction patterns of the synthesized composites were obtained by powder X-ray diffraction (XRD, D/Max 2550V, Rigaku, Japan), using Cu Kα radiation (λ = 1.5418 Å). Chemical and elemental analyses were used to quantitatively measure the composition of the composite. Transmission

electron microscopy (TEM), high-resolution transmission microscopy (HRTEM, JEM 2010, JEOL, Japan) and scanning electron microscope (SEM, JSM-6700F, JEOL, Japan) were used to observe the microstructure of the composites. Energy-dispersive spectroscopy (EDS) was also taken on the same apparatus as TEM. The electrical conductivities of the composites were measured by the Hall effect measurement system (HL5500PC, UK). Electrochemical measurements of sintered CNT–TiN samples were performed with a standard three-electrode electrochemical cell. This system consisted of a CNT–TiN pellet as the working electrode, a Pt foil as the counter electrode, and a saturated calomel electrode (SCE) as the reference electrode. The electrolytes included an aqueous solution of 0.1 M H₂SO₄, 0.1 M KCl, or 0.1 M KCl + 10⁻³ M KOH. The electrochemical experiments were controlled by a ZF-3 potentiostat and ZF-4 potential scanner.

Results and discussion

Zeta potential studies of the pristine, acid-treated CNTs and treated CNTs in the presence of the Ti precursor are shown in Fig. 1. After acid treatment, the isoelectric point (pH_{iep}) of the CNTs moves to a more acidic value, with the zeta potential values being more negative. The changes must be due to the existence of acidic groups on the surface of the CNTs.¹ The addition of the Ti precursor increases the zeta potential values for all pH values studied, which means that the Ti precursor can adsorb onto the treated CNTs in the entire experimental range. Fig. 2 illustrates XPS spectroscopy of treated CNTs in the presence of the Ti precursor. The Ti 2p peak at 460 eV is observed, which is considered as evidence for the adsorption of the Ti precursor at the surface of the CNTs.

To investigate the adsorption mechanism of the Ti precursor on the CNTs, FTIR spectra are shown in Fig. 3. The bands at 1715 and 1580 cm⁻¹ of treated CNTs are assigned to stretching vibrations of C=O and COO⁻, respectively. From curve (b), the spectrum of the CNT–Ti precursor shows peaks at 1457 and 1376 cm⁻¹ corresponding to asymmetric and symmetric stretching vibrations of carboxylate. In addition, the band attributed to the stretching of C=O moves to 1626 cm⁻¹. It can be suggested that good chemical absorption between modified CNTs and the Ti precursor is formed, which enhances interfacial combination between the above two components

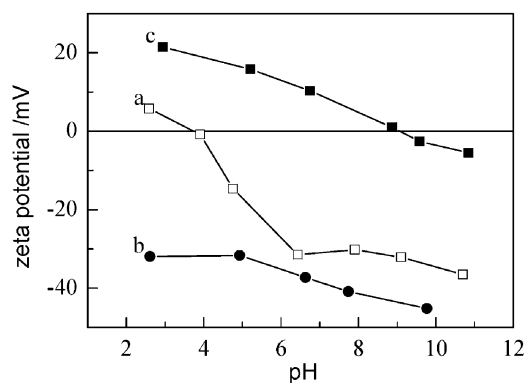


Fig. 1 Zeta potential values changed with pH of: (a) pristine CNTs; (b) acid-treated CNTs; (c) a mixture of treated CNTs and Ti precursor.

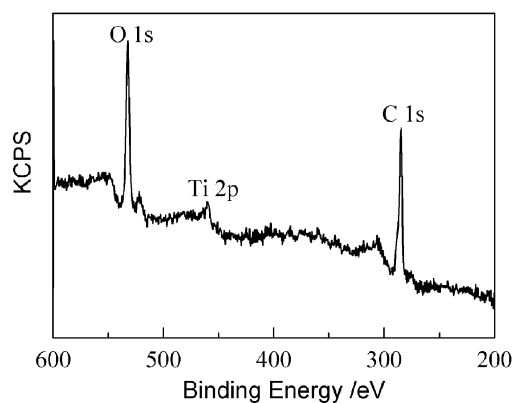


Fig. 2 XPS spectra of treated CNTs in the presence of the Ti precursor.

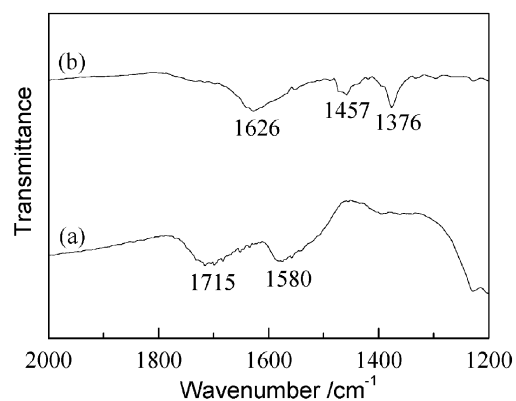


Fig. 3 FTIR spectra of: (a) acid-treated CNTs; and (b) the mixture of CNTs and Ti precursor.

and improves the dispersion ability of the nanotubes in the as-obtained nitride matrix. Acid treatment on the nanotubes can improve the dispersion ability of the CNTs in a medium and activate their chemically inert surfaces.^{10,23} In addition, the structure of the titanium precursor employed in this report entails the –OH group, which is beneficial to interact with the acid groups on the CNTs.

The CNT–TiN composites obtained after nitridation were determined using XRD, as shown in Fig. 4. The XRD peaks correspond well with the reported values of TiN (JCPDS 87–0682) in curve (b). The peak at 26.06° is attributed to the characteristic peaks of the CNTs. Moreover, chemical and elemental analyses quantitatively confirm the formation of the CNT–TiN composite. The analyses found (calculated) are, in wt%: Ti, 70.66 (73.31); N, 19.57 (21.45); C, 5.19 (5.24). The calculated contents of CNTs in the composite are obtained according to the original addition of the nanotubes. The measured values correspond well with those calculated, which indicates relatively high purity of the synthesized composites and little loss of CNTs in the fabrication process of the composite.

The difference in electrical conductivity between the CNT–nitride composite and the neat nitride material was measured according to the standard four-point probe technique. The

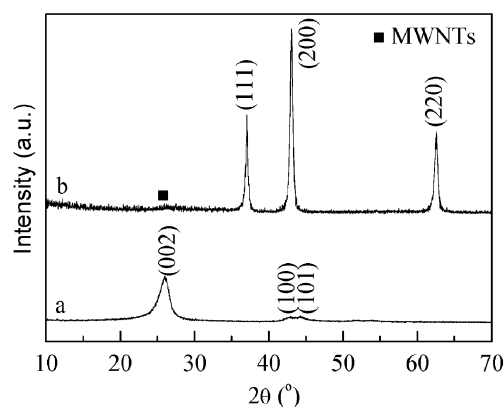


Fig. 4 XRD patterns of: (a) CNTs; and (b) CNT–TiN nanocomposites nitrided at 800 °C for 5 h in an NH₃ atmosphere.

resistivity (ρ) of TiN and the CNT–TiN composite was measured to be 0.00197 and 0.00136 Ωcm , respectively (Table 1). Thus the conductivity (σ) for each was calculated to be 508 and 735 S cm^{-1} , respectively. By adding about 12 vol% CNTs, the electrical conductivity of the CNT–TiN composite is increased by about 45% compared to that of TiN.

Microstructure investigation of the CNT–TiN composite is needed to explain how the CNTs increase the electrical conductivity of TiN. The morphologies of the CNT–TiN composites were examined by TEM, HRTEM, and SEM, as shown in Fig. 5. The typical micrograph in Fig. 5a clearly shows that tiny TiN nanoparticles are well attached to the CNTs, with a diameter of *ca.* 5–10 nm. To investigate the composition of these nanoparticles, EDS measurement was performed. The EDS spectrum (shown in the inset of Fig. 5a) indicates that these tiny particles anchored on the nanotubes consist of TiN. The oxygen peak found in the spectrum may be attributed to the oxygen-containing groups on the acid-treated CNTs. The lattice fringe spacing of the attached nanocrystal is indexed as the (200) plane of the TiN reflection in Fig. 5b. After calcination of the precursor in a protective atmosphere, tiny TiO₂ nanoparticles were firstly yielded on the nanotubes. Then during the following nitridation process, tiny TiN nanoparticles were produced *in situ* on the CNTs. In addition, because of the restriction effect of CNTs on the growth of attached particles,²⁴ the diameter of the TiN nanoparticles attached on the nanotubes is only several nanometers, much smaller than bulk particles which are mostly in the range of *ca.* 15–25 nm in Fig. 5c. According to XRD analysis, the calculated average size of the bulk particles is about 20 nm, which is in good agreement with the results of TEM observation.

Table 1 Properties of the investigated materials

System	$\sigma/\text{S cm}^{-1}$ [$\rho/\Omega\text{cm}$]		CNT content (vol%)	Increase in σ (%)
	Neat nitride	CNT–nitride		
TiN system	508 [0.00197]	735 [0.00136]	12.4	44.7
Fe ₂ N system	794 [0.00126]	885 [0.00113]	11.7	11.5

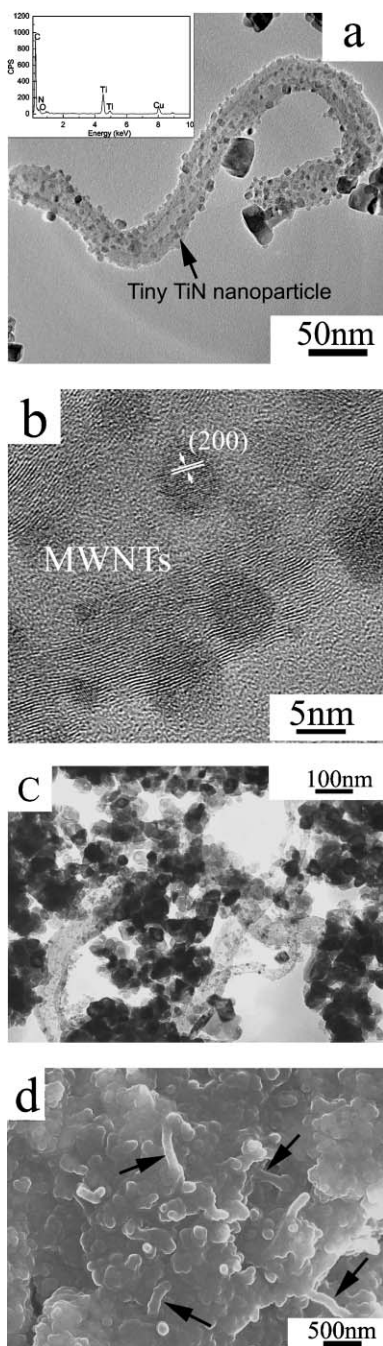


Fig. 5 Micrographs of the CNT–TiN nanocomposite: (a) TEM image showing TiN nanoparticles attached onto the CNTs, with a diameter of *ca.* 5–10 nm, the EDS spectrum of the attached nanoparticles is shown in the inset; (b) HRTEM image showing TiN nanoparticles attached onto the CNTs; (c) good dispersion of TiN nanoparticle-anchored CNTs within the TiN powder; (d) the arrows in the SEM image point to several CNTs connecting TiN conducting domains.

An SEM micrograph used to investigate the surface of the CNT–TiN composite is shown in Fig. 5d. The SEM observations show: (i) that CNTs are separately dispersed in the TiN matrix; (ii) that CNTs locate at the boundary of the TiN grains; (iii) that CNTs may be wetted by the matrix; and

(iv) that CNT acts as a bridge to connect the different domains of the matrix. Moreover, TEM images show that the surfaces of the CNTs are coated with tiny TiN nanoparticles, which is important for enhancing the properties of the composite (a detailed discussion is shown in the next paragraph). Previous studies^{7,25,26} have proved that CNTs, which show these microstructures, could act to reinforce the mechanical or electrical properties of the composites. For this new CNT–TiN composite, we primarily measured its electrical properties compared with those of the CNT-free composite. For the mechanical properties, such as stiffness, fracture strength, and fracture toughness, modest improvements have been reported for CNT–metal oxide composites.^{25,27} However, some studies did not provide the expected enhancement in mechanical properties for the CNT-containing composites due to the lower relative densities or lower volume fraction of CNTs in the composites.^{7,28} Our initial work on the measurement of stiffness for this new CNT–TiN composite shows little improvement compared with the CNT-free composite, probably due to the same reasons.^{7,28} A lot of work is needed to further study the mechanical properties of this new class of CNT–nitride composites.

From TEM and SEM micrographs, it is observed that the surface of the CNT is modified by tiny TiN nanoparticles. The structure of tiny TiN-anchored CNTs will play an important role in the fabrication and enhanced electrical properties of the composite. On one hand, the adhesion of TiN nanoparticles to the CNTs overcomes the van der Waals interaction between the nanotubes, which generally otherwise would result in CNT aggregates or bundles.⁴ Hence, a relatively good dispersion of the nanotubes in the TiN matrix is obtained (Fig. 5c and d). On the other hand, the TiN-anchored nanotube is in favor of good adhesion and strengthened interfacial combination to the bulk matrix. The attached TiN nanoparticles provide a favourable interface to promote the combination between the CNTs and the TiN matrix, and a good interfacial combination is a significant factor for improving the properties of the composite.^{7,23}

How the CNTs enhance the electrical conductivity of the composite may be attributed to two reasons. One reason is the introduction of effective conducting paths to the TiN, *viz.*, the percolation effect of the CNTs.^{7,29} Previous researches have shown that the free path to carry conduction electrons is an important factor affecting the electrical properties of TiN, and the conduction electron scatters at the grain boundaries.¹³ The CNT, as a good conducting path,^{1,4} is located at the grain boundaries of the composite, as derived from the microstructure investigation. The presence of CNTs at the grain boundaries strengthens the carrier transport ability, and thus enhances the electrical conductivity of the composite. Another important microscopic feature derived from the SEM micrograph is that the CNTs may serve as a conducting bridge to connect TiN conductible domains. This bridge-connected function also promotes the charge mobility of the CNT–TiN composite over that of TiN. The other reason is a good interfacial combination between CNTs and the matrix. The tiny TiN nanoparticles attached on CNT wall serve as a good interface between the CNTs and the matrix in the sintered composite, and an enhanced cohesion

between the CNTs and the TiN matrix is produced. Thus an effective electron transfer from the matrix to the nanotube is realized. Hence, in the presence of 12 vol% CNTs, the CNT–TiN composite exhibits a 45% increase in electrical conductivity over TiN.

The electrochemical behavior of the TiN and CNT–TiN composite was recorded using cyclic voltammetry (CV) technology. Fig. 6 compares a typical cyclic voltammogram for CNT–TiN nanocomposite to that of TiN. In 0.1 M H₂SO₄, 0.1 M KCl, or 0.1 M KCl + 10^{−3} M KOH CV electrolyte solution, the voltammograms of these two materials have very similar shaped CV curves, and no clear electroactivity could be observed in the observed potential ranges. It can be seen that the addition of CNTs would not change the electrochemical stability of the TiN material. Janes *et al.*¹⁵ pointed out that

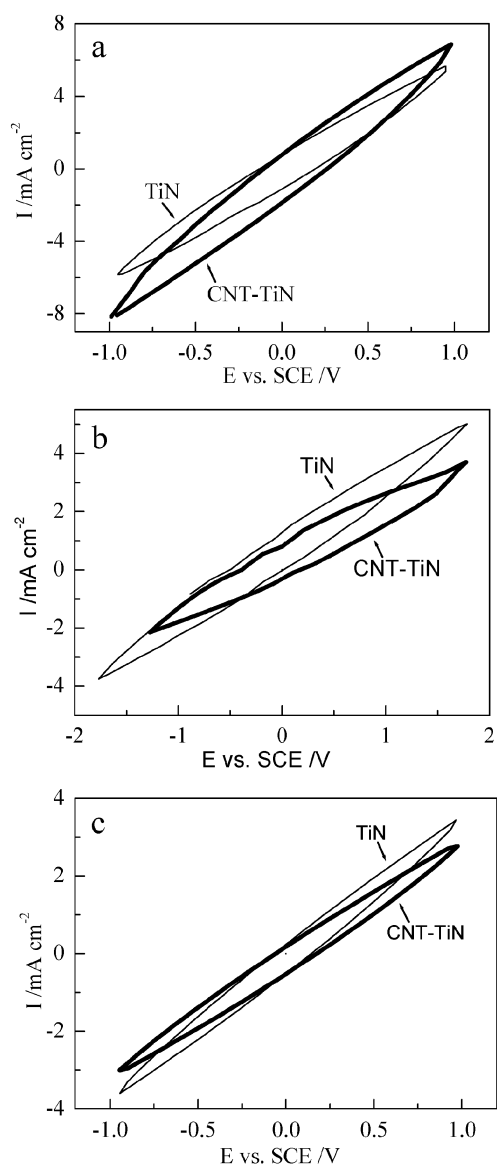


Fig. 6 Cyclic voltammogram of TiN and CNT–TiN composites: (a) in an aqueous solution of 0.1 M H₂SO₄; (b) in an aqueous solution of 0.1 M KCl; (c) in an aqueous solution of 0.1 M KCl + 10^{−3} M KOH. Potential scan rate = 200 mV s^{−1}.

the electrochemical stability, corrosion resistance and high conductivity of TiN make it an excellent candidate for electrodes in electrochemical capacitors, which use highly corrosive electrolytes such as KOH. The CNT–TiN composite fabricated in this report effectively improves the electrical conductivity without altering the electrochemical stability of TiN in highly corrosive electrolytes, which is expected to promote the application of the TiN material in electrochemical capacitors.

In addition, we also fabricated the CNT–Fe₂N composite and measured its electrical conductivity. The XRD peaks are consistent with the reported values of Fe₂N (JCPDS 06–0656), as shown in curve (b) of Fig. 7. The characteristic peak of CNTs exists at $2\theta = 26.06^\circ$. The form of the composite was quantitatively measured by chemical and elemental analyses. The analyses found (calculated): Fe, 84.61 (84.52); N, 10.60 (10.60); C, 4.20% (4.88%). The measured values are close to the calculated ones due to the high purity of the composite and little loss of CNTs in the fabrication process of the CNT–Fe₂N composite. In the presence of about 12 vol% CNTs, the electrical conductivity of the CNT–Fe₂N composite is increased by a slight improvement of 12% over that of Fe₂N from 794 to 885 S cm^{−1}, as shown in Table 1. The increase in the electrical conductivity of CNT–Fe₂N is much lower than that of CNT–TiN. TEM, HRTEM and SEM micrographs of the CNT–Fe₂N sintered material are illustrated in Fig. 8. In the CNT–Fe₂N composite, the microstructure of the Fe₂N-attached CNT does not exist in Fig. 8a. The CNT bundles are aggregated around the large Fe₂N particles with diameters of several hundred nanometers. The lattice fringe spacing of the nanoparticle is indexed as the (002) plane of the Fe₂N reflection in Fig. 8b. The magnified micrograph of the CNT aggregate in the composite is shown in the inset of Fig. 8c. Comparing Fig. 5d and Fig. 8c, it is obvious that the CNT–Fe₂N composite shows serious aggregation of CNTs bundles in the matrix. A slight increase of electrical property in CNT–Fe₂N is owed to the percolation effect of the CNTs to Fe₂N. However, serious aggregation of CNTs in the matrix greatly restricts the further improvement in electrical property. The absence of nitride-attached CNT microstructure leads to a poor interfacial adhesion between CNTs and the Fe₂N matrix. This phenomenon corresponds well

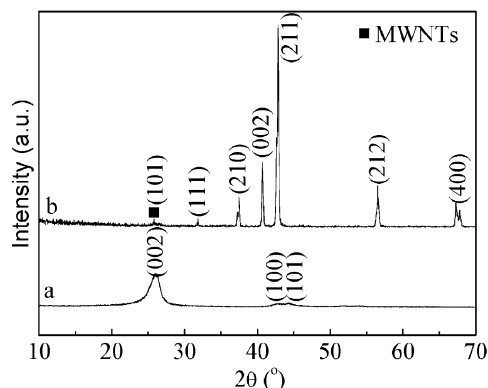


Fig. 7 XRD patterns of: (a) CNTs; and (b) CNT–Fe₂N nanocomposites nitrided at 800 °C for 5 h in an NH₃ atmosphere.

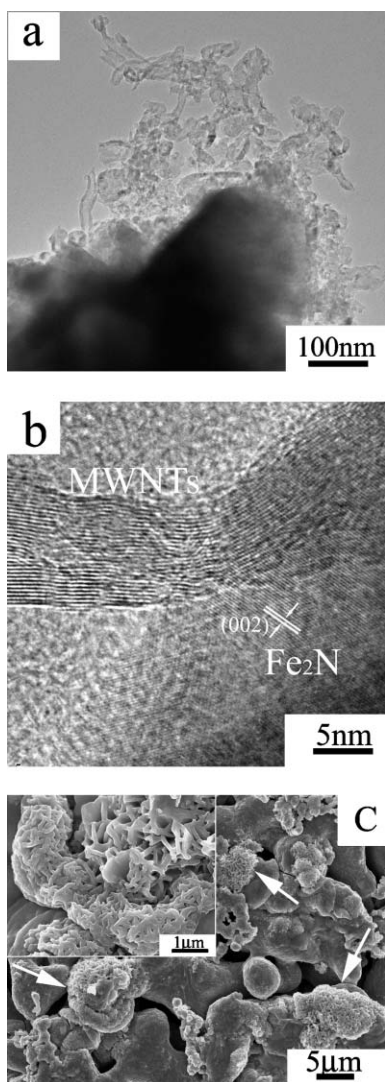


Fig. 8 (a) TEM image and (b) HRTEM image of the CNT-Fe₂N composite; (c) SEM image of the CNT-Fe₂N composite after sintering, which shows comparatively poor dispersion of the CNTs in the matrix. The arrows in the image point to several CNT great aggregates in the composite. For clarification, the magnified image of the CNT aggregate in the matrix by the arrows is shown in the inset.

with the above conclusion, which demonstrates that the nitride-attached CNT would play an important role on the enhanced composite properties.

Conclusions

New CNT-TiN and CNT-Fe₂N nanocomposites with enhanced electrical properties were successfully fabricated. In the presence of 12 vol% CNTs, the CNT-TiN composite exhibits a 45% increase in electrical conductivity over that of the TiN material. The addition of CNTs still retains the original electrochemical stability of TiN, which makes the composite an excellent candidate for electrodes in electrochemical capacitors. The fabrication of tiny TiN nanoparticles attached on individual CNTs promotes good dispersion of the CNTs in the composite and facilitates interfacial adhesion

between the CNTs and the nitride matrix. Without such nanoparticle-attached microstructures, the CNT-Fe₂N composite only shows 12% improvement in electrical property by adding about 12 vol% CNTs. The introduction of conducting paths by CNTs and the bridge-connected function of CNTs between the conducting domains are possible mechanisms leading to the improvement of the electrical conductivity. CNT-nitride composites, as a new class of material with enhanced electrical properties, may have potential applications in CNT-based nanoelectronic industries, electrochemical capacitor production and other important fields.

Acknowledgements

Authors thank for the support from National Nature Science Foundation of China (No. 50372077) and Shanghai Nanotechnology Promotion Center (No. 0252nm025). The authors thank Dr Y. Z. Zhang for her hearty assistance in acquiring CV data. The authors thank Ms M. L. Ruan for her help in acquiring TEM and HRTEM images.

Linquin Jiang^{ab} and Lian Gao^{*ab}

^aState Key Laboratory of High Performance Ceramics and Superfine Microstructure, Shanghai Institute of Ceramics, Chinese Academy of Sciences, Shanghai, 200050, P. R. China. E-mail: liangaoc@online.sh.cn; Fax: 0086 21 52413122; Tel: 0086 21 52412718

^bGraduate School of the Chinese Academy of Sciences, Shanghai, 200050, P. R. China

References

- G. Z. Chen, M. S. Shaffer, D. Coleby, G. Dixon, W. Zhou, D. J. Fray and A. H. Windle, *Adv. Mater.*, 2000, **12**, 522.
- J. Sandler, M. S. P. Shaffer, T. Prasse, W. Bauhofer, K. Schulte and A. H. Windle, *Polymer*, 1999, **40**, 5967.
- W.-Q. Han and A. Zettl, *Nano Lett.*, 2003, **3**, 681.
- H. Zengin, W. Zhou, J. Jin, R. Czerw, D. W. Smith, Jr., L. Echegoyen, D. L. Carroll, S. H. Foulger and J. Ballato, *Adv. Mater.*, 2002, **14**, 1480.
- A. Peigney, Ch. Laurent and A. Rousset, *Key Eng. Mater.*, 1997, **132-136**, 743.
- L. Xu, B. Q. Wei, R. Z. Ma, J. Liang, X. K. Ma and D. H. Wu, *Carbon*, 1999, **37**, 855.
- E. Flahaut, A. Peigney, Ch. Laurent, Ch. Marlière, F. Chastel and A. Rousset, *Acta Mater.*, 2000, **48**, 3803.
- P. M. Ajayan and Q. Z. Zhou, *Top. Appl. Phys.*, 2001, **80**, 391.
- P. G. Collins and P. Avouris, *Sci. Am.*, 2000, **283**, 62.
- C. N. R. Rao, B. C. Satishkumar, A. Govindaraj and M. Nath, *ChemPhysChem*, 2001, **2**, 78.
- A. Peigney, E. Flahaut, Ch. Laurent, F. Chastel and A. Rousset, *Chem. Phys. Lett.*, 2002, **352**, 20.
- L. Q. Jiang and L. Gao, *Chem. Mater.*, 2003, **15**, 2848.
- P. Patsalalas and S. Logothetidis, *J. Appl. Phys.*, 2001, **90**, 4725.
- C. J. Carmalt, S. R. Whaley, P. S. Lall, A. H. Cowley, R. A. Jones, B. G. McBurnett and J. G. Ekerdt, *J. Chem. Soc., Dalton Trans.*, 1998, 553.
- R. A. Janes, M. Aldissi and R. B. Kaner, *Chem. Mater.*, 2003, **15**, 4431.
- Il-S. Kim and P. N. Kumta, *J. Mater. Chem.*, 2003, **13**, 2028.
- M. S. Cao, R. G. Wang, X. Y. Fang, Z. X. Cui, T. J. Chang and H. J. Yang, *Powder Technol.*, 2001, **115**, 96.
- Q. Liang, B. C. Liu, S. H. Tang, Z. J. Li, Q. Li, L. Z. Gao, B. L. Zhang and Z. L. Yu, *Acta Chim. Sin.*, 2000, **58**, 1336.
- J. Y. Chen, L. Gao and J. H. Huang, *J. Mater. Sci.*, 1996, **31**, 3497.
- Y. Qiu and L. Gao, *Mater. Res. Bull.*, 2003, **38**, 1551.

-
- 21 R. B. Penland, S. Mizushima, C. Curran and J. V. Quagliano, *J. Am. Chem. Soc.*, 1957, **79**, 1575.
- 22 O. Carp, L. Patron, L. Diamandescu and A. Reller, *Thermochim. Acta*, 2002, **390**, 169.
- 23 R. Andrews, D. Jacques, D. L. Qian and T. Rantell, *Acc. Chem. Res.*, 2002, **35**, 1008.
- 24 P. Chen, X. Wu, J. Lin and K. L. Tan, *J. Phys. Chem. B*, 1999, **103**, 4559.
- 25 J. Sun, L. Gao and W. Li, *Chem. Mater.*, 2002, **14**, 5169.
- 26 G.-D. Zhang, J. Kuntz, J. Wan and A. K. Mukherjee, *Nature Mater.*, 2003, **2**, 38.
- 27 R. Z. Ma, J. Wu, B. Q. Wei, J. Liang and D. H. Wu, *J. Mater. Sci.*, 1998, **33**, 5243.
- 28 Ch. Laurent, A. Peigney, O. Dumortier and A. Rousset, *J. Eur. Ceram. Soc.*, 1998, **18**, 2005.
- 29 E. Kymakis, I. Alexandou and G. A. J. Amaratunga, *Synth. Met.*, 2002, **127**, 59.